Sensors & Actuators: A. Physical 371 (2024) 115272

Contents lists available at ScienceDirect

Sensors and Actuators: A. Physical

journal homepage: www.journals.elsevier.com/sensors-and-actuators-a-physical

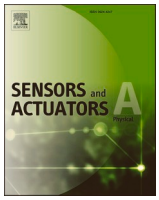

Exploring the contraction actuation of magnetically functionalized electrospun tubes

Vincenzo Iannotti [a,b,*,1], Vincenzo Guarino [c,1], Iriczalli Cruz-Maya [c], Zaheer Ud Din Babar [d], Luca Lanotte [e], Luigi Ambrosio [c], Luciano Lanotte [a,c]

[a] Department of Physics "E. Pancini", University of Naples Federico II, Piazzale V. Tecchio 80, Naples 80125, Italy
[b] CNR-SPIN (Institute for Superconductors, Oxides and Other Innovative Materials and Devices), Piazzale V. Tecchio 80, Naples 80125, Italy
[c] Institute of Polymers, Composites and Biomaterials (IPCB) National Research Council of Italy, Mostra d'Oltremare Pad. 20, V.le J. F. Kennedy 54, Naples 80125, Italy
[d] Scuola Superiore Meridionale (SSM), University of Naples Federico II, Largo S. Marcellino 10, Naples 80138, Italy
[e] UMR STLO, INRAE, Institut Agro Rennes-Angers, Rennes 35000, France

ARTICLE INFO

Keywords:
Magneto-active devices
Contraction actuators
Biomedical application
Magneto-elastic sensors

ABSTRACT

Recently, magnetically functionalized polymer tubes (MFPTs) have been fabricated through a multistep electrospinning process. These innovative MFPTs can serve as ducts suitable for microfluidic components and biomedical devices. Considering these applications, it is crucial to investigate the effectiveness of inducing oscillating contractions at low frequencies. For this purpose, we designed an experimental setup to study the cross-sectional contraction of these smart tubes when subjected to a magnetic field produced by the oscillation of a small permanent magnet. A magnetoelastic wave resonator placed near the MFPT section detects the induced contraction, enabling the calculation of both its magnitude and response times. The results demonstrate that oscillating contractions, resulting in a maximum reduction of duct radius by approximately 43%, can be achieved with an oscillating magnetic induction field of amplitude around 10 mT, at a low frequency not exceeding 1/2 Hz. These findings highlight the potential of such innovative MFPTs, particularly in the fields of surgery and endoscopy.

1. Introduction

In recent years, the use of smart devices composed of magnetic charges dispersed in various configurations (uniformly or localized) within a flexible matrix has increased significantly. These devices have wide applications in micromechanical and biomedical fields, serving purposes such as neural probes, microneedles, micro-pumps for insulin delivery, intraocular and inner ear drug delivery systems, and fluid pumps [1–15]. Magnetic actuators generally offer precise control and high performance [16]. For instance, a small magnet placed between two flexible polyimide membranes was used to achieve moderate displacement (ranging from 0 to 0.05 mm) in response to an external magnetic field (4–30 mT) for 1-second time [17]. More frequently, a combination of micro- or nanoparticles within a polymer matrix, such as biocompatible polydimethylsiloxane, is utilized to produce magneto-rheological elastomer sheets, that exhibit deflections or notable changes in resistivity when subject to an applied magnetic field [18–22]. In the wake of these pioneering studies, there have been significant advancements in the production of electrospun fibers, greatly contributing to the production of advanced functional materials [23–27]. Tubular electrospun devices are becoming increasingly important in biotechnology [28] and many biomedical applications [29–31]. These applications range from prostheses designed to support various tissues and organs, such as blood vessels [32], intestines [33], peripheral nerves [34], tendons [35,36], and bones [37], to antimicrobial catheters [38]. Furthermore, substantial efforts have been directed towards the development of smart polymer tubes capable of offering versatile and complex deformations for use in applications such as robotic manipulation [39], displacement actuators [40], shape recovery components [41], and pH control [42].

In the context of this research topic, in a previous investigation we focused on the fabrication and characterization of elastomagnetic nanostructured tubes made of polycarbonate-urethane nanofibers with embedded nickel (Ni) nanoparticles [43]. We optimized the process for incorporating and dispersing magnetic particles in the fibers while

* Corresponding author at: Department of Physics "E. Pancini", University of Naples Federico II, Piazzale V. Tecchio 80, Naples 80125, Italy.
E-mail address: vincenzo.iannotti@unina.it (V. Iannotti).
[1] These authors contributed equally to this work.

https://doi.org/10.1016/j.sna.2024.115272
Received 3 December 2023; Received in revised form 4 March 2024; Accepted 11 March 2024
Available online 16 March 2024

considering the role of particle size and aggregation in the device functionalities. These nanostructured tubes exhibited remarkable properties, including significant longitudinal strain under a moderate magnetic field. Based on previous studies that combined a magnetic field with the electrospinning process [44], we developed a configuration that allowed us to align magnetic nanofibers along the line of the maximum magnetic force intensity. This results in the formation of nanofibrous wires with a high density of magnetic nanoparticles [45], which is crucial for achieving substantial elastomagnetic deflection and elongation useful for applications in electromechanical and biomedical devices. Additionally, we explored recent developments in producing programmed and aligned filament-like fibers [46] using various external assistance methods during electrospinning, even in a cylindrical configuration [47].

In our recent studies, we achieved significant improvements in magnetic smart devices with tube-shaped designs. Specifically, we developed nanocomposite tubes that incorporated a thin longitudinally oriented ribbon of magnetic nanofibers localized along the lateral surface of the tube [48]. This innovative structure results in tubes that undergo substantial transverse contraction, with a tube eccentricity of over 50% and radius decreasing by 40% along the axis of an external magnetic field. These effects were achieved with a moderate magnetic stimulus characterized by a magnetizing field gradient of $\leq$30 mT/mm at a basic intensity of $<$ 40 mT.

These newly developed magnetically functionalized polymer tubes (MFPTs) can play a crucial role in meeting the demand for tubular devices capable of inducing transverse strains. Such devices have the potential to address common issues in biomedicine, such as obstructions, and serve as microelectromechanical flow regulators. In this state-of-the-art study, the primary objective was to characterize the dynamic response of the newly produced MFPTs under an alternate magnetic field. First, we investigated the correlation between the contraction levels and the static external magnetic field. Subsequently, we characterized the dependence of the actuated contraction on an alternating magnetizing field, revealing the potential and limitations of MFPTs in generating oscillating contractions at low frequencies. The miniaturization of the investigated tubular devices and their possible implementation with elastic membranes opens up new and exciting possibilities in biomedical and microfluidic applications, as discussed in the conclusions.

2. Experimental methods

2.1. MFPT characterization

The MFPTs were fabricated via electrospinning, as reported elsewhere [48]. Here, for brevity, we will directly provide a summary of the sample morphology along with the essential geometry data. The core of the production process involves electrospinning a solution of polycarbonate-urethane (PCU) and magnetic nanoparticles (MNPs) onto a pre-deposited pure PCU tube. The magnetic ribbon consists of an electrospun mat of polycarbonate-urethanes (PCU) (Chorethane 80 A) nanofibers, which includes Ni nanoparticles (99,99% Aldrich Chemical) serving as a magnetic filler at a concentration of 12% v/v relative to the polymer. A previous investigation showed that the average nanofiber diameter is 2.2 μm, and the nanoparticles are below 200 nm in size [48]. The MFPTs used in this study were cut to a fixed length of 20 mm.

Fig. 1 displays the cross-section of the samples with the average value of key parameters such as D (vertical diameter), L (horizontal diameter), *l* (width of magnetic nanofiber mat (MNM) electrospun on the top side of the tube), t (thickness of MNM), s (average thickness of the tube wall), and s' (wall thickness on the inside and outside of the mat). The weight-induced strain effect is evident, reducing D and increasing L when viewing the cross-section in a vertical plane with the MNM on the top.

2.2. Apparatus and methodology for actuating static and oscillating transverse strain

To apply a magnetic field with a defined intensity and gradient to the MFPTs, we used a cylindrical NdFeB permanent magnet (PM; 3 mm in diameter and 5 mm in height). The B_0 magnetic induction field along the magnet axis versus the distance from its polar surface was measured using a standard Hall Probe, and it is shown in Fig. 2. When the MNM piece was exposed to the PM field (inset of Fig. 2), the Ni nanoparticles inside the nanofiber developed a magnetic moment (m_s) along the x-

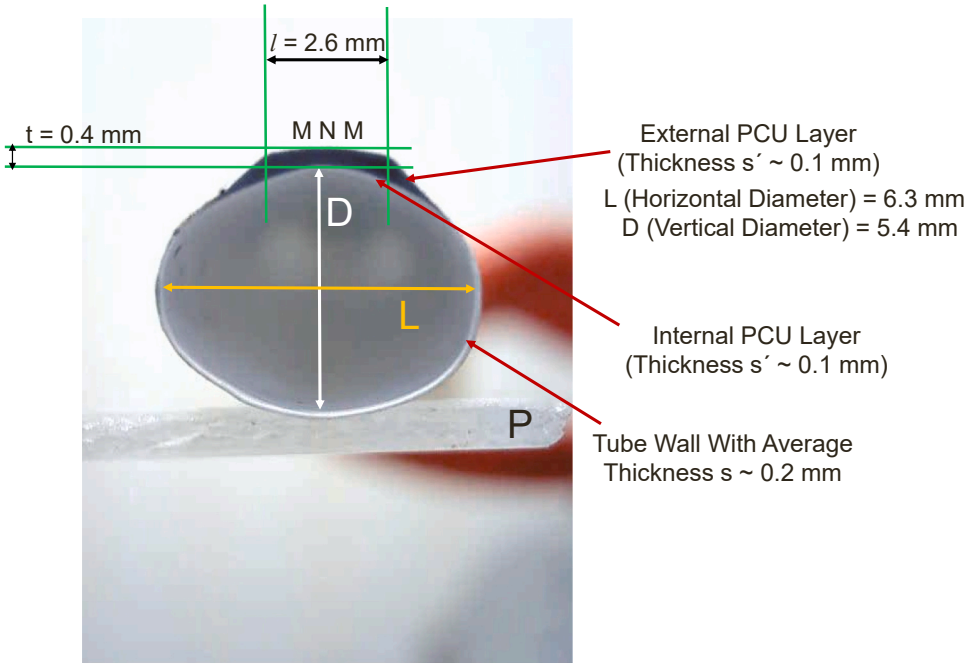

Fig. 1. Cross-section of the magnetically functionalized polymer tubes placed on a 1.2 mm thick plexiglass support P, with the MNM in a horizontal plane. Photographs were captured using a TESLONG MS 100 optical magnification camera.

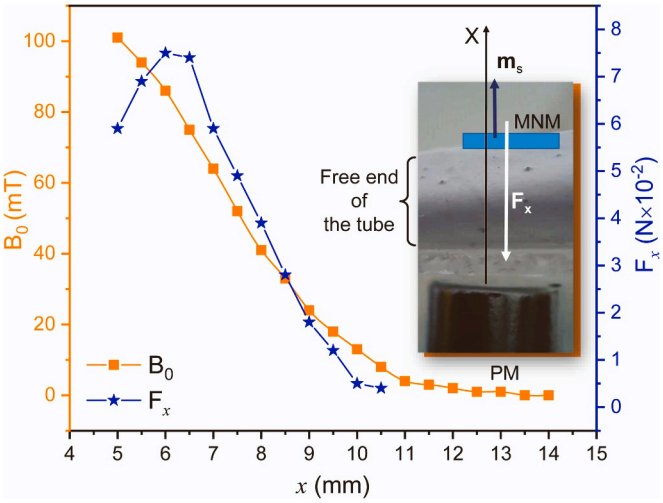

Fig. 2. The orange curve (square dots) illustrates the variation of the B_0 magnetic induction field along the axis of the PM as a function of the distance (x) from the polar surface. The photo in the inset shows the action of the magnet on the MNM positioned towards one end of the MFPT and its consequent contraction. In blue (star dots), the behaviour of the force acting on the MNM, which induces the cross-section contraction of the MFPT, is depicted based on the simplified model producing Eq. (5).

axis, simultaneously generating a magnetic force

$$F_x = m_s\, \partial B_0/\partial x \tag{1}$$

that pulled the magnetized MNM on the top side of the tube toward the magnet. As a result of F_x, the MNM displaces towards the region of higher magnetic field intensity, causing concurrent deformation (as seen in the crushed cross-section of the tube in Fig. 3**(a), and (b)**). Notably, the magnetic force did not uniformly strain the MFPT because the magnetic action was concentrated at one end of the tube segment used in the experiment. Consequently, the elastic response of the polymer nanocomposite tube is not symmetrical on either side of F_x (see the inset of Fig. 2, where the MNM's left side shows the tube segment's end, while the right side displays a longer portion of the tube). The displacement not only leads to deformation but also enhances F_x because the magnetized MNM approaches regions of a higher magnetic induction field as it moves.

Considering the magnetic force component in Eq. (1), we can assume that the magnetic moment (m_s) is the product of the magnetization intensity in the Ni particles (M) and the volume of the MNM portion affected by the magnetization ($\Delta\tau$), reduced to 12% (percentage occupied by the nickel particles):

$$m_s = M\ \Delta\tau\ 12\% \tag{2}$$

M is determined as:

$$M = (\mu_r/\mu_0)\ B_0 \tag{3}$$

where μ_r, μ_0, and B_0 are the relative magnetic permeability, the absolute magnetic permeability of the vacuum, and the magnetic induction field, respectively.

Therefore, Eq. (1) becomes:

$$F_x = m_s\, \partial B_0/\partial x = M\ \Delta\tau\ 12\%\ \partial B_0/\partial x = (\mu_r/\mu_0)\ B_0\ \Delta\tau\ 12\%\ \partial B_0/\partial x \tag{4}$$

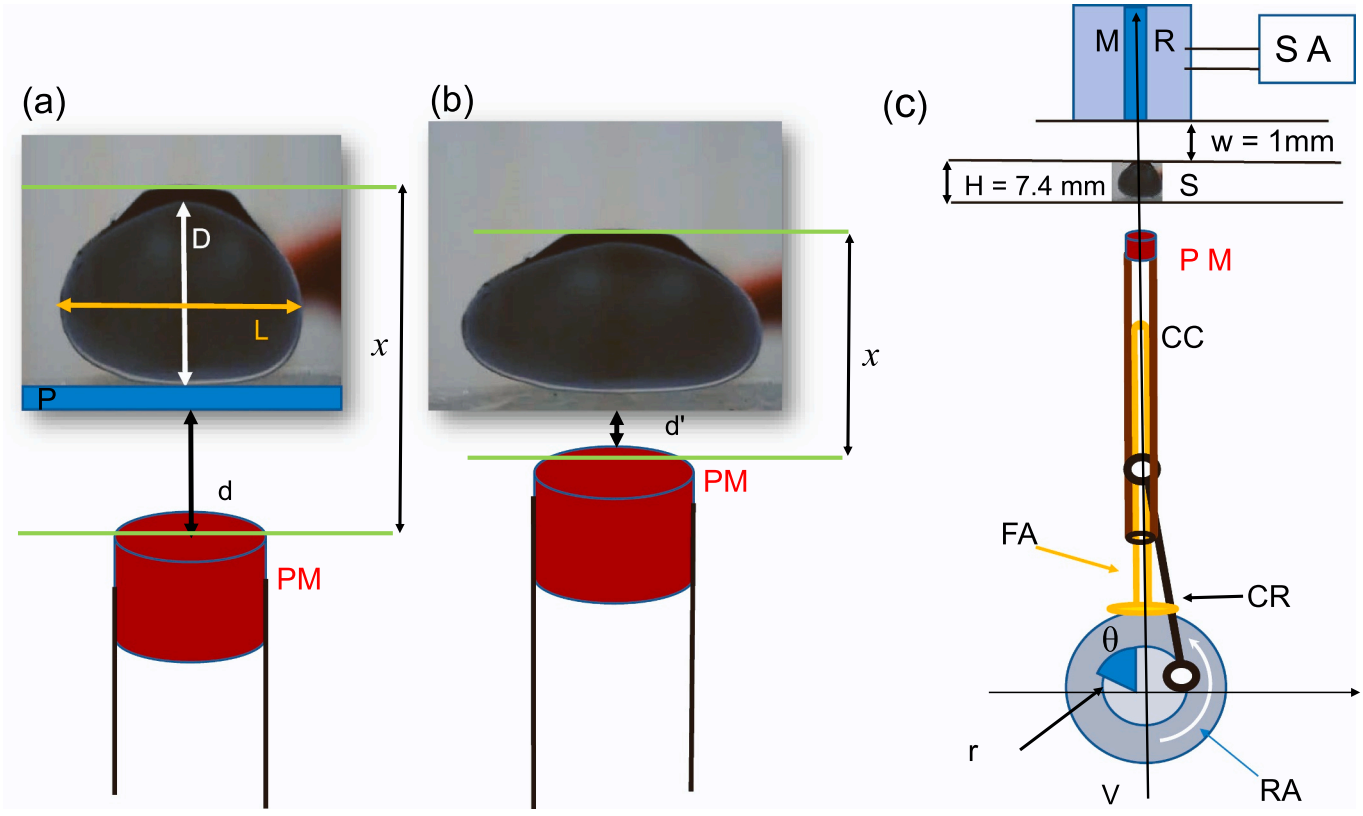

Fig. 3. MFPT contraction study: Magnetic force-induced deformation and experimental setup. (a) MFPT cross-section when the PM is distant (d > 3 mm) from the plexiglass support P. (b) MFPT cross-section when the PM is near (d < 3 mm) to the plexiglass support P. In particular, the specific photo refers to d= 4.5 mm and d'= 0.7 mm, the minimum distance recorded during the experiment. (c) Experimental apparatus scheme: MR = Magnetoelastic resonator; SA= Signal Analyzer; S = sample; PM = permanent magnet; CC = cursor; FA = fixed rod on which CC slides; CR = Connecting rod; RA = rotating apparatus; θ = rotation angle; r = distance from the axis of rotation of the CR; w = 1 mm is the distance between MR and MNM in the zero-contraction condition.

Considering that the average relative permeability from transversal magnetization measurements on MNM is approximately $\mu_r \approx 200$ (between 10 mT and 70 mT) and that the MNM volume directly in front of the permanent magnet is $\Delta\tau = 0.4 \bullet 2.6 \bullet 3.0\ mm^3 \approx 3.1 \bullet 10^{-9}\ m^3$, Eq. (4) can be expressed as:

$$F_x \approx 59 \bullet 10^{-3}\ (A\ m^2/T) \bullet B_0 \bullet \partial B_0/\partial x \quad (5)$$

By utilizing the calibration curve (Fig. 2) to determine, for each x value, both B_0 and its derivative with respect to x, Eq. (5) enables to approximate calculation of the force acting along the x-axis, pulling the end of the MFPT towards the magnet. The trend of this force is depicted by the blue line in Fig. 2. It is evident that the actuating mechanism is capable of generating a total force equivalent to a few grams, reaching its maximum at a distance of approximately 6 mm from the MNM.

To further investigate, we employed a highly sensitive sensor to detect changes in the local induction magnetic field (B) and monitor the strain induced on the MFPTs at a fixed position. For this purpose, we utilized a magnetoelastic resonator (MR) featuring a sensitive core composed of an amorphous metal strip with high initial magnetic susceptibility [49]. The MR has proven effective in monitoring both static and dynamic displacements and oscillations [50–52].

The experimental setup illustrated in Fig. 3**(c)** was designed for the production, detection, and characterization of the magnetically actuated transverse contraction of the MFPTs under static and dynamic conditions. The monitored sample section 'S' is positioned such that its diameter D is aligned with the vertical axis. The MR is located coaxially above S, whereas the PM is below it. The PM can be moved toward or away from the sample or oscillated at a low frequency using the telescoping cursor CC, which slides on the fixed cylindrical axis FA. The sliding motion is driven by a connecting rod CR controlled by a rotor RA. The rotor can be turned manually using a micrometer knob or rotated at a fixed angular speed using a motor (with a frequency ranging from 0 to 3 Hz). The connecting rod is engaged at a distance r from the axis of rotation. Because the length of the connecting rod is 50 mm and r = 3 mm, it can be demonstrated that the displacement of the slider's end, measured from its topmost position, is approximately equal to r − r cos (θ), where θ is the angle formed by r with the vertical axis (see Fig. 3**(c)**).

3. Experiment modeling, results, and discussion

The magnetoelastic resonator is sensitive to the local axial magnetic field because an increase in this field reduces the amplitude of the resonant magnetoelastic waves in its core sensor. This occurs because the resonance condition is initially established at the peak of the magnetic permeability of the amorphous ribbon core. Therefore, an increase in axial magnetization leads to a decrease in magnetic permeability, subsequently reducing the amplitude of the magneto-elastic waves.

Fig. 4 illustrates the calibration curve of the MR, representing the magnetoelastic wave amplitude (A_0) versus the distance d. This experimentally detected data is presented under two different conditions: in the presence of fields produced by PM+MNM (triangle dots), and when the MFPT is removed, causing changes in the magnetizing field due only to the PM displacement (circle dots). In these measurements, the distance (d) from the magnet to plexiglass support P was statically changed using a micrometric cursor, enabling an excursion greater than that in the dynamic oscillating condition (> 6 mm). As the parameter d changes, Fig. 4 reveals that A_0 remain unaffected by the presence of MNM when d > 6.7 mm. A decrease is noted when d falls below 6.7 mm, consistent with expectations that the MNM's magnetization intensifies the magnetic field acting on the MR.

However, as d decreases to less than 3.7 mm, the rate of decrease diminishes. This effect arises from tube contraction, displacing the magnetized ribbon (MNM) away from the sensor (MR), thus reducing the local magnetic field on the MR. Additionally, below 3 mm, the greater contraction of the tube in the presence of MNM leads to a larger

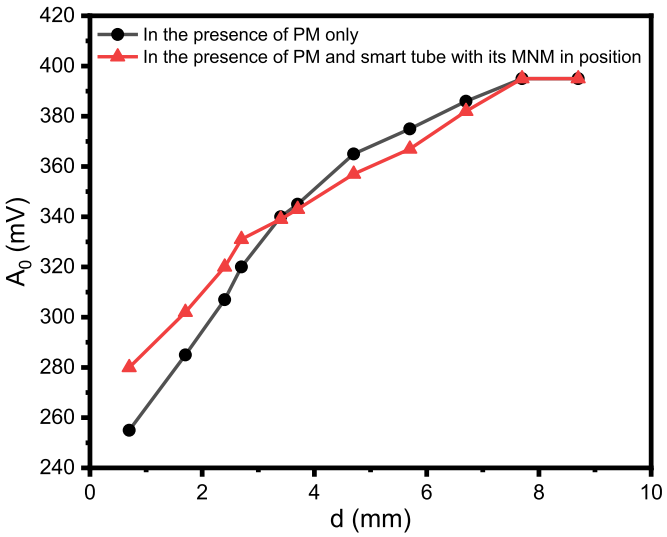

Fig. 4. Amplitude of the magnetoelastic waves detected by MR as a function of the distance d between the PM and the base of the plexiglass support P (see Fig. 3). The circle dots represent measurements obtained when only the PM field is present, while the triangle dots correspond to measurements taken with the smart tube and its MNM in position, as depicted in Fig. 3. The reported values were obtained from 10 repeated runs (increasing and decreasing d), with an experimental error of ± 1 mV.

Ao compared to the corresponding value observed without MNM.

In the experimental configuration shown in Fig. 3, it is important to note that the cursor has a total stroke of 6 mm. To prevent contact with the plexiglass base, the minimum value of d was 0.7 mm. Based on the interpretation provided, Fig. 4 suggests that the MFPT contracts significantly when d values range from 0.7 mm to 2.7 mm.

As shown in **Movie.S1**, shifting the PM closer to the pipe in static positions, initially from a distance of approximately d ≈ 3 mm and moving downwards, gradually increases the section's contraction, reducing the D diameter. Fig. 5 provides a detailed representation of the trend of A_0 in relation to d, compared to the corresponding variation in diameter D for the range 0.7 mm < d < 3.0 mm. The D value decreases from approximately 43% to 4%. The values at the experimental points remained consistent across repeated measurement cycles (increasing and decreasing d), falling within the instrumental measurements error of ± 1 mV for A_0 and ± 0.1 mm for d and D. This result suggests the possibility of indirectly obtaining D values from measurements of the amplitude A_0, using the corresponding curves in Fig. 5. In principle, since the measurement of the amplitude A_0 has an instrumental percentage error (0.3–0.4%) smaller than that of the diameter dimension D (2–3%), it is evident that performing an indirect evaluation of the contraction through the measurement of A_0 allows for greater sensitivity than direct measurement. A limitation lies in the fact that the experimental trends are not linear. Consequently, to obtain corresponding values in unmeasured conditions, linear interpolation between the known values of both A_0 and D must be considered valid. However, the indirect estimation of D through the measurement of A_0 is particularly suitable for online monitoring of the impact of magnetic fields that vary slowly enough to induce actual contraction of the tubes.

Consequently, after calibrating the experimental system and conducting static checks to evaluate the shrinkage effect of the new polymeric tubes under an external magnetic field, the focus of this investigation shifted to implementing and detecting the contraction under dynamic conditions. Specifically, this involves applying an alternating magnetic field with a variable frequency.

The magnetic field was generated by alternately moving the PM, controlled by the rotating apparatus shown in Fig. 3, at low frequencies ≤ 3 Hz. Fig. 6 shows the displacement Y (black line) over time for 1 Hz

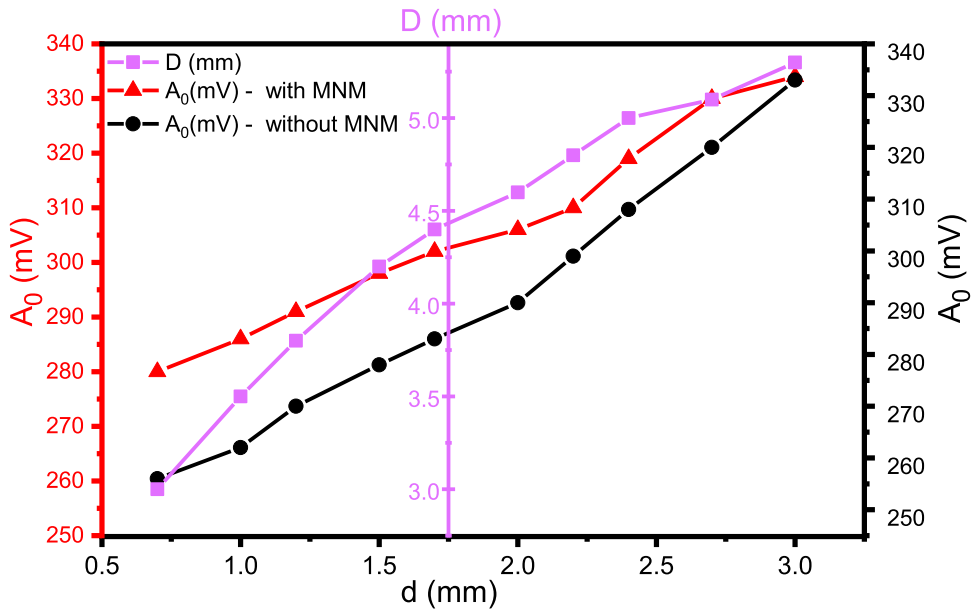

Fig. 5. Behavior of A_0 compared with the corresponding behavior of D (vertical diameter of the sample cross-section parallel to the applied magnetic field), as d changes. Square dots represent the D values. Triangle dots represent A_0 values in the presence of the MFPT, while circle dots denote measurements obtained when the sample is absent.

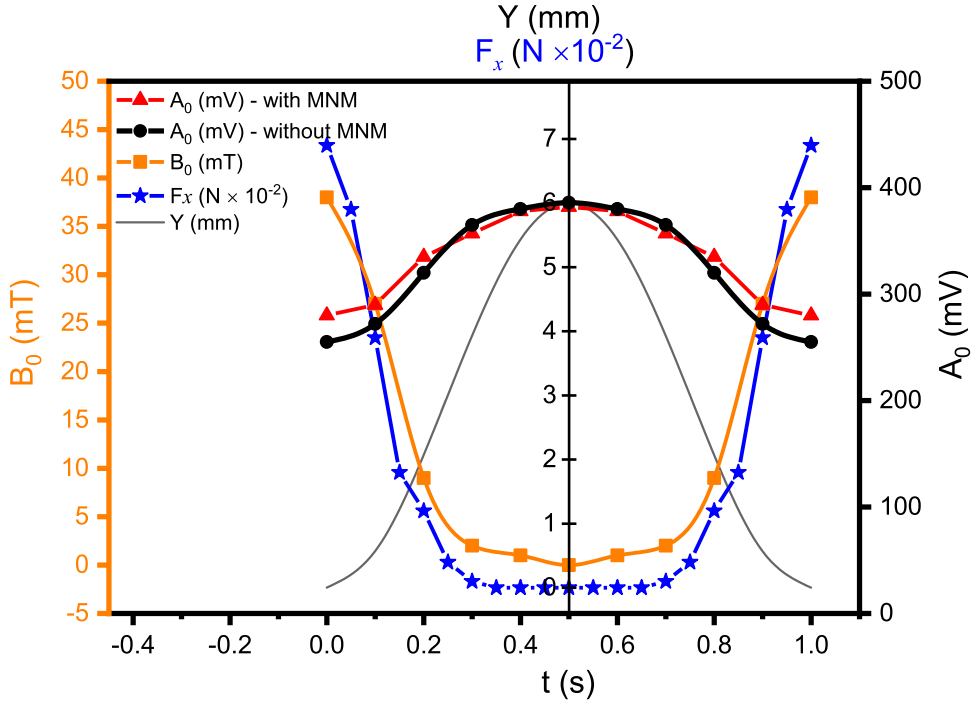

Fig. 6. Simulation of the magnet displacement (Y) versus time (t) (black line) during one complete oscillation at a frequency of 1 Hz, correlated with the corresponding magnetic induction field (B_0) (square dots), actuating force F_x (star dots), and magnetoelastic wave amplitude (A_0) versus displacement. A_0 is depicted under conditions without MNM (circle dots) and with MNM (triangle dots).

oscillations under the most favorable conditions, where the minimum distance (d=0.7 mm) is achieved. The same figure includes the corresponding B_0 field value (square dots) obtained from the calibration curve in Fig. 2. Additionally, it displays the expected amplitude (A_0) of the magnetoelastic waves, derived from the calibration curves reported in Fig. 5, both in presence (triangle dots) and absence (circle dots) of MNM. Upon careful examination of the trends in Fig. 6, it becomes evident that a nearly cosine-shaped oscillation of the actuator magnet displacement (black line) does not correspond to an equally harmonic B_0 field trend applied to the nanofiber mat (square dots). This discrepancy is mainly due to the significant field decay that occurs as the magnet moves further away. The variation in amplitude of the resonant magnetoelastic waves, depicted by the circle dots without MNM and the triangle dots with MNM, was more pronounced at shorter distances, gradually diminishing as the distances increased. Furthermore, the comparison of the magnetoelastic wave amplitude (A_0) without MNM and with MNM aligns with the behavior of the actuating force F_x (star dots in Fig. 6), calculated using Eq. (5) for x values corresponding to the

magnet displacement and adjusted so as to take into account the contraction of D illustrated in Fig. 5. Notably, in Fig. 6, the increasing separation of the A_0 curves, indicating the deformation of the MFPT cross-section, correspond to the growth of the actuating force F_x responsible for this deformation.

The experimental trend of the modulation of the magnetoelastic wave amplitude, in presence of the MNM, is visualized in Fig. 7 for PM oscillations at frequencies of 1/3, 1/2, and 1 Hz. It is evident that A_0 exhibits the expected rapid decay as the magnet approaches the MNM. Furthermore, as the frequency exceeds 1/2 Hz, the A_0 value decreases more than in quasi-static measurements (1/3 Hz). This indicate that tube contraction does not reach its complete excursion. In other words, the behavior of A_0 versus t suggests that the MNM has negligible displacement.

In essence, if the step (Δ) between higher and lower A_0 values in the modulation induced by alternate magnetization is 131 mV (matching the circle dots curve in Fig. 6), it indicates the absence of contraction. Conversely, if this step reduces to 102 mV, as observed in the triangle dots curve in Fig. 6, it signifies that contraction has reached its optimal excursion.

In Fig. 8, the behavior of Δ versus frequency in the range from 0.2 Hz to 1 Hz is presented. One can observe the progressive increase of Δ (indicating constriction abatement) starting from 0.5 Hz up to 1 Hz. The uncertainty in repeated measurements was kept within ± 0.05 Hz for frequency and ± 1 mV for Δ.

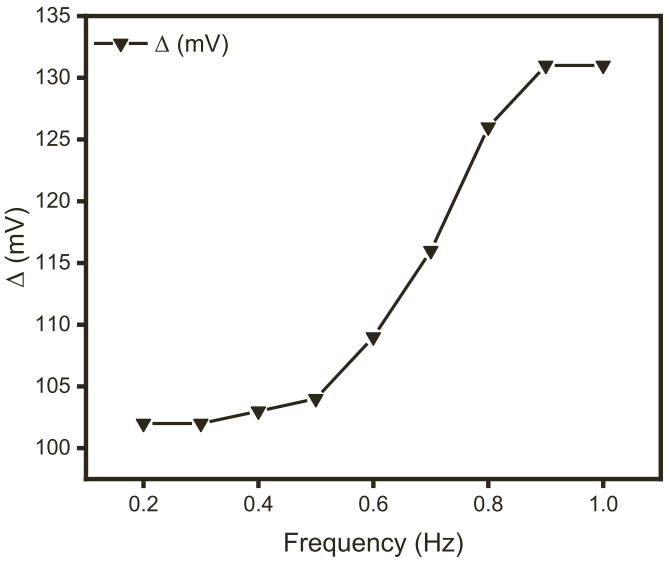

Fig. 8. Variation in the Step (Δ) between higher and lower A_0 values in the modulation induced by the alternate magnetizing field as the frequency ranges from 0.2 Hz to 1 Hz.

4. Conclusions

In this investigation, we present a range of experimental results that enhance our understanding of magnetically actuated transverse contraction in recently developed nanostructured polymer tubes. The significance of these findings can be summarized as follows:

I. A simple mechanical apparatus, specifically designed and constructed for this purpose, enables the oscillating contraction of MFPT at a low frequency without direct contact.
II. Our experiment revealed that the cross-sectional contraction of the new MFPT occurred in response to the magnetic field of a small PM, resulting in a contraction ranging from 4% to 43%. This behavior was experimentally confirmed by the MR data, as depicted in Fig. 5.
III. By using the static calibration curve of PM (axial magnetic induction field versus distance; Fig. 2) in combination with the MR's static calibration curve (illustrating the magnetoelastic wave amplitude A_0 versus distance from the PM in both absence and presence of MNM; Fig. 5), we can simulate the expected behavior of A_0 during oscillating contraction, highlighting its correlation with the force generated by the actuating alternate magnetizing field (Fig. 6).
IV. Our experiments directly detected A_0 and confirmed its expected behavior, particularly at low frequencies (Fig. 7). Moreover, the complete set of experimental (Fig. 8) and simulated data under dynamic conditions allows us to conclude that the contraction begins to be incomplete at frequencies above 1/2 Hz. In other words, due to the viscoelastic response of the complex MFPT structure, their oscillating contraction is actuated only for oscillation periods exceeding 2 s.

Overall, these findings reveal the promising smart properties of new MFPTs, with vast potential applications across a spectrum of fields. Specifically, these materials offer innovative solutions for resolving occlusive phenomena in small- or medium-caliber conduit substitutes, which are critical in vascular prostheses [53], cardiology [54], as well as in the urinary [55], biliary [56], bowel [57], lacrimal [58], and esophagogastic [59] ducts, and the insertion of guidewires and probes [60]. Considering successful applications involving compression induced by magnets [61] and magnetically induced vibrations in metal elements [62] that have already emerged, the most significant advantage of the new MFPTs is the elimination of the need for metal parts or internal magnets in the body, thus ensuring patient safety.

Beyond the biomedical context, these tubes also offer substantial advantages for controlling fluid flow in conduits, particularly in microelectromechanical devices such as fluid flow gates [63]. Their unique properties, including elasticity, deformability, and conductivity, make them versatile for various applications, including flexible sensors and piezoelectric devices [64,65]. In summary, magnetically functionalized polymer tubes represent a groundbreaking development with a

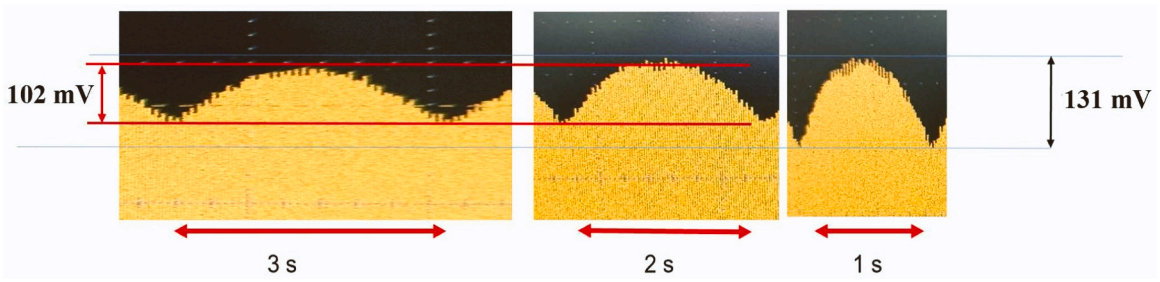

Fig. 7. Modulation of the magnetoelastic wave amplitude due to the periodic magnetizing field generated by the oscillating permanent magnet at frequencies of 1/3 Hz (on the left), 1/2 Hz (center), and 1 Hz (on the right). The amplitude of the A_0 modulation in the absence of tube contraction (131 mV) is shown on the right, while on the left is the corresponding value (102 mV) when contraction occurs as effectively as in static conditions.

wide range of potential applications, marking a significant step toward innovative and minimally invasive solutions in various fields.

CRediT authorship contribution statement

Luciano Lanotte: Writing – review & editing, Supervision, Project administration, Methodology, Conceptualization. **Luigi Ambrosio:** Supervision. **Vincenzo Guarino:** Writing – original draft, Visualization, Methodology, Investigation, Conceptualization. **Vincenzo Iannotti:** Writing – original draft, Validation, Methodology, Investigation, Formal analysis, Conceptualization. **Zaheer Ud Din Babar:** Writing – review & editing, Visualization, Data curation. **Iriczalli Cruz-Maya:** Visualization, Investigation, Data curation. **Luca Lanotte:** Writing – review & editing, Validation, Formal analysis.

Declaration of Competing Interest

The authors declare that they have no known competing financial interests or personal relationships that could have appeared to influence the work reported in this paper.

Data Availability

Data will be made available on request.

Appendix A. Supporting information

Supplementary data associated with this article can be found in the online version at doi:10.1016/j.sna.2024.115272.

References

[1] H. Fallahi, J. Zhang, H.P. Phan, N.T. Nguyen, Flexible microfluidics: Fundamentals, recent developments, and applications, Micromachines 10 (2019) 830, https://doi.org/10.3390/mi10120830.

[2] S. Mondal, N. Zehra, A. Choudhury, P.K. Iyer, Wearable sensing devices for point of care diagnostics, ACS Appl. Bio Mater. 4 (2021) 47–70, https://doi.org/10.1021/acsabm.0c00798.

[3] A. Cobo, R. Sheybani, H. Tu, E. Meng, A wireless implantable micropump for chronic drug infusion against cancer, Sens. Actuators, A Phys. 239 (2016) 18–25, https://doi.org/10.1016/j.sna.2016.01.001.

[4] M. Tahmasebipour, A.A. Paknahad, Unidirectional and bidirectional valveless electromagnetic micropump with PDMS-Fe3O4 nanocomposite magnetic membrane, J. Micromech. Microeng. 29 (2019) 075014, https://doi.org/10.1088/1361-6439/ab1dbe.

[5] M.M. Said, J. Yunas, B. Bais, A.A. Hamzah, B.Y. Majlis, The design, fabrication, and testing of an electromagnetic micropump with a matrix-patterned magnetic polymer composite actuator membrane, Micromachines 9 (2018) 13, https://doi.org/10.3390/mi9010013.

[6] M. Ashouri, M.B. Shafii, A. Moosavi, Theoretical and experimental studies of a magnetically actuated valveless micropump, J. Micromech. Microeng. 27 (2017) 015016, https://doi.org/10.1088/0960-1317/27/1/015016.

[7] J. Zhang, J. Xu, J. Lim, J.K. Nolan, H. Lee, C.H. Lee, Wearable glucose monitoring and implantable drug delivery systems for diabetes management, Adv. Healthc. Mater. 10 (2021) 2100194, https://doi.org/10.1002/adhm.202100194.

[8] P. Gurman, O.R. Miranda, K. Clayton, Y. Rosen, N.M. Elman, Clinical applications of biomedical microdevices for controlled drug delivery, Mayo Clin. Proc. 90 (2015) 93–108, https://doi.org/10.1016/j.mayocp.2014.10.003.

[9] H. Zhang, J.K. Jackson, M. Chiao, Microfabricated drug delivery devices: design, fabrication, and applications, Adv. Funct. Mater. 27 (2017) 1–31, https://doi.org/10.1002/adfm.201703606.

[10] C. Wang, J. Park, Magnetic micropump embedded in contact lens for on-demand drug delivery, Micro Nano Syst. Lett. 8 (2020) 4–9, https://doi.org/10.1186/s40486-019-0101-x.

[11] S.H. Lee, Y.Bin Lee, B.H. Kim, C. Lee, Y.M. Cho, S.N. Kim, C.G. Park, Y.C. Cho, Y. Bin Choy, Implantable batteryless device for on-demand and pulsatile insulin administration, Nat. Commun. 8 (2017) 1–10, https://doi.org/10.1038/ncomms15032.

[12] N.A. Hamid, B.Y. Majlis, J. Yunas, A.R. Syafeeza, Y.C. Wong, M. Ibrahim, A stack bonded thermo-pneumatic micro-pump utilizing polyimide based actuator membrane for biomedical applications, Microsyst. Technol. 23 (2017) 4037–4043, https://doi.org/10.1007/s00542-016-2951-y.

[13] M.W. Becker, J.A. Simonovich, E.A. Phelps, Engineered microenvironments and microdevices for modeling the pathophysiology of type 1 diabetes, Biomaterials 198 (2019) 49–62, https://doi.org/10.1016/j.biomaterials.2018.07.002.

[14] A. Abbas, C. Zhang, M. Asad, A. Waqas, A. Khatoon, S. Hussain, S.H. Mir, Recent developments in artificial super-wettable surfaces based on bioinspired polymeric materials for biomedical applications, Polymers 14 (2022) 238, https://doi.org/10.3390/polym14020238.

[15] Y. Zhang, A.D. Mickle, P. Gutruf, L.A. McIlvried, H. Guo, Y. Wu, J.P. Golden, Y. Xue, J.G. Grajales-Reyes, X. Wang, S. Krishnan, Y. Xie, D. Peng, C.J. Su, F. Zhang, J.T. Reeder, S.K. Vogt, Y. Huang, J.A. Rogers, R.W. Gereau, Battery-free, fully implantable optofluidic cuff system for wireless optogenetic and pharmacological neuromodulation of peripheral nerves, Sci. Adv. 5 (2019) 1–12, https://doi.org/10.1126/sciadv.aaw5296.

[16] D. Chouhan, S. Mehrotra, O. Majumder, B.B. Mandal, Magnetic actuator device assisted modulation of cellular behavior and tuning of drug release on silk platform, ACS Biomater. Sci. Eng. 5 (2019) 92–105, https://doi.org/10.1021/acsbiomaterials.8b00240.

[17] S. Imai, T. Tsukioka, A magnetic MEMS actuator using a permanent magnet and magnetic fluid enclosed in a cavity sandwiched by polymer diaphragms, Precis. Eng. 38 (2014) 548–554, https://doi.org/10.1016/j.precisioneng.2014.02.003.

[18] C. Wang, S.J. Seo, J.S. Kim, S.H. Lee, J.K. Jeon, J.W. Kim, K.H. Kim, J.K. Kim, J. Park, Intravitreal implantable magnetic micropump for on-demand VEGFR-targeted drug delivery, J. Control. Release 283 (2018) 105–112, https://doi.org/10.1016/j.jconrel.2018.05.030.

[19] M.M. Schmauch, S.R. Mishra, B.A. Evans, O.D. Velev, J.B. Tracy, Chained iron microparticles for directionally controlled actuation of soft robots, ACS Appl. Mater. Interfaces 9 (2017) 11895–11901, https://doi.org/10.1021/acsami.7b01209.

[20] M. Manzo, M. Bakaraju, Novel thin polymeric magnetic membranes study for applications in the future biomedical devices, AIP Adv. 12 (2022) 115221, https://doi.org/10.1063/5.0130683.

[21] P.R. von Lockette, S.E. Lofland, J.H. Koo, J. Kadlowec, M. Dermond, Dynamic characterization of bimodal particle mixtures in silicone rubber magnetorheological materials, Polym. Test. 27 (2008) 931–935, https://doi.org/10.1016/j.polymertesting.2008.08.007.

[22] L. Lanotte, G. Ausanio, C.L. Hison, V. Iannotti, L. Lanotte, Magneto-piezoresistance in elastomagnetic composites, J. Appl. Phys. 110 (2011) 063903, https://doi.org/10.1063/1.3634120.

[23] D. Blond, W. Walshe, K. Young, F.M. Blighe, U. Khan, D. Almecija, L. Carpenter, J. McCauley, W.J. Blau, J.N. Coleman, Strong, tough, electrospun polymer-nanotube composite membranes with extremely low density, Adv. Funct. Mater. 18 (2008) 2618–2624, https://doi.org/10.1002/adfm.200701487.

[24] C. Huang, S.J. Soenen, J. Rejman, J. Trekker, L. Chengxun, L. Lagae, W. Ceelen, C. Wilhelm, J. Demeester, S.C. De Smedt, Magnetic electrospun fibers for cancer therapy, Adv. Funct. Mater. 22 (2012) 2479–2486, https://doi.org/10.1002/adfm.201102171.

[25] C. Chen, J. Tang, Y. Gu, L. Liu, X. Liu, L. Deng, C. Martins, B. Sarmento, W. Cui, L. Chen, Bioinspired hydrogel electrospun fibers for spinal cord regeneration, Adv. Funct. Mater. 29 (2019) 1–11, https://doi.org/10.1002/adfm.201806899.

[26] L. Zhang, W. Yu, C. Han, J. Guo, Q. Zhang, H. Xie, Q. Shao, Z. Sun, Z. Guo, Large scaled synthesis of heterostructured electrospun TiO 2 / SnO 2 nanofibers with an enhanced photocatalytic activity, J. Electrochem. Soc. 164 (2017) H651–H656, https://doi.org/10.1149/2.1531709jes.

[27] Y. Guo, X. Yang, K. Ruan, J. Kong, M. Dong, J. Zhang, J. Gu, Z. Guo, Reduced graphene oxide heterostructured silver nanoparticles significantly enhanced thermal conductivities in hot-pressed electrospun polyimide nanocomposites, ACS Appl. Mater. Interfaces 11 (2019) 25465–25473, https://doi.org/10.1021/acsami.9b10161.

[28] N. Pien, I. Peeters, L. Deconinck, L. Van Damme, L. De Wilde, A. Martens, S. Van Vlierberghe, P. Dubruel, A. Mignon, Design and development of a reinforced tubular electrospun construct for the repair of ruptures of deep flexor tendons, Mater. Sci. Eng. C. 119 (2021) 111504, https://doi.org/10.1016/j.msec.2020.111504.

[29] N. Moazeni, M. Vadood, D. Semnani, H. Hasani, Modeling the compliance of polyurethane nanofiber tubes for artificial common bile duct, Mater. Res. Express 5 (2018) 025004, https://doi.org/10.1088/2053-1591/aaa77e.

[30] I.A. Fiqrianti, P. Widiyanti, M.A. Manaf, C.Y. Savira, N.R. Cahyani, F.R. Bella, Poly-L-Lactic acid (PLLA)-chitosan-collagen electrospun tube for vascular graft application, J. Funct. Biomater. 9 (2018) 32, https://doi.org/10.3390/jfb9020032.

[31] M.Q. Khan, D. Kharaghani, N. Nishat, Sanaullah, A. Shahzad, T. Yamamoto, Y. Inoue, I.S. Kim, In vitro assessment of dual-network electrospun tubes from poly (1,4 cyclohexane dimethylene isosorbide terephthalate)/PVA hydrogel for blood vessel application, J. Appl. Polym. Sci. 136 (2019) 47222, https://doi.org/10.1002/app.47222.

[32] B. Zavan, C. Gardin, V. Guarino, T. Rocca, I.C. Maya, F. Zanotti, L. Ferroni, G. Brunello, J.C. Chachques, L. Ambrosio, V. Gasbarro, Electrospun pcl-based vascular grafts: In vitro tests, Nanomaterials 11 (2021) 1–16, https://doi.org/10.3390/nano11030751.

[33] S.R. Son, R.A. Franco, S.H. Bae, Y.K. Min, B.T. Lee, Electrospun PLGA/gelatin fibrous tubes for the application of biodegradable intestinal stent in rat model, J. Biomed. Mater. Res. - Part B Appl. Biomater. 101B (2013) 1095–1105, https://doi.org/10.1002/jbm.b.32923.

[34] V. Cirillo, B.A. Clements, V. Guarino, J. Bushman, J. Kohn, L. Ambrosio, A comparison of the performance of mono- and bi-component electrospun conduits in a rat sciatic model, Biomaterials 35 (2014) 8970–8982, https://doi.org/10.1016/j.biomaterials.2014.07.010.

[35] O. Evrova, G.M. Bürgisser, C. Ebnöther, A. Adathala, M. Calcagni, E. Bachmann, J. G. Snedeker, C. Scalera, P. Giovanoli, V. Vogel, J. Buschmann, Elastic and surgeon friendly electrospun tubes delivering PDGF-BB positively impact tendon rupture

healing in a rabbit Achilles tendon model, Biomaterials 232 (2020) 119722, https://doi.org/10.1016/j.biomaterials.2019.119722.
[36] G. Meier Bürgisser, M. Calcagni, A. Müller, E. Bonavoglia, G. Fessel, J.G. Snedeker, P. Giovanoli, J. Buschmann, Prevention of peritendinous adhesions using an electrospun DegraPol polymer tube: A histological, ultrasonographic, and biomechanical study in rabbits, Biomed. Res. Int. 2014 (2014) 656240, https://doi.org/10.1155/2014/656240.
[37] V. Cirillo, V. Guarino, L. Ambrosio, Design of bioactive electrospun scaffolds for bone tissue engineering, J. Appl. Biomater. Funct. Mater. 10 (2012) 223–228, https://doi.org/10.5301/JABFM.2012.10343.
[38] Y.K. Chao, C.H. Lee, K.S. Liu, Y.C. Wang, C.W. Wang, S.J. Liu, Sustained release of bactericidal concentrations of penicillin in the pleural space via an antibiotic-eluting pigtail catheter coated with electrospun nanofibers: Results from in vivo and in vitro studies, Int. J. Nanomed. 10 (2015) 3329–3336, https://doi.org/10.2147/IJN.S82228.
[39] Y. Wang, J. Liu, D. Zhu, H. Chen, Active tube-shaped actuator with embedded square rod-shaped ionic polymer-metal composites for robotic-assisted manipulation, Appl. Bionics Biomech. 2018 (2018) 4031705, https://doi.org/10.1155/2018/4031705.
[40] M.Y. Razzaq, M. Balk, M. Mazurek-Budzyńska, A. Schadewald, From nature to technology: exploring bioinspired polymer actuators via electrospinning, Polymers 15 (2023) 4029, https://doi.org/10.3390/polym15194029.
[41] S.L. Buffington, J.E. Paul, M.M. Ali, M.M. Macios, P.T. Mather, J.H. Henderson, Enzymatically triggered shape memory polymers, Acta Biomater. 84 (2019) 88–97, https://doi.org/10.1016/j.actbio.2018.11.031.
[42] V. Mansard, A macroporous smart gel based on a pH-sensitive polyacrylic polymer for the development of large size artificial muscles with linear contraction, Soft Matter 17 (2021) 9644–9652, https://doi.org/10.1039/d1sm01078f.
[43] V. Guarino, G. Ausanio, V. Iannotti, L. Ambrosio, L. Lanotte, Electrospun nanofiber tubes with elastomagnetic properties for biomedical use, Express Polym. Lett. 12 (2018) 318–329, https://doi.org/10.3144/expresspolymlett.2018.28.
[44] Y. Wu, J. Yu, J. He, Y.-Q. Wan, Controlling stability of the electrospun fiber by magnetic field, Chaos, Solitons & Fractals 32 (2007) 5–7, https://doi.org/10.1016/j.chaos.2006.05.023.
[45] V. Guarino, V. Iannotti, G. Ausanio, L. Ambrosio, L. Lanotte, Elastomagnetic nanofiber wires by magnetic field assisted electrospinning, Express Polym. Lett. 13 (2019) 419–428, https://doi.org/10.3144/expresspolymlett.2019.35.
[46] A.A. Lach, H.L. Morris, J.A. Martins, E.T. Stace, A.J. Carr, P.A. Mouthuy, Pyridine as an additive to improve the deposition of continuous electrospun filaments, PLoS One 14 (2019) 1–16, https://doi.org/10.1371/journal.pone.0214419.
[47] Y. Li, C. Zhang, L.F. Zhu, Z. Ahmad, J.S. Li, M.W. Chang, Elastic antibacterial membranes comprising particulate laden fibers for wound healing applications, J. Appl. Polym. Sci. 136 (2019) 1–9, https://doi.org/10.1002/app.47105.
[48] V. Guarino, V. Iannotti, G. Ausanio, L. Ambrosio, L. Lanotte, Nanocomposite tubes for magneto-active devices, Express Polym. Lett. 14 (2020) 651–662, https://doi.org/10.3144/expresspolymlett.2020.53.
[49] L. Lanotte, G. Ausanio, M. Carbucicchio, V. Iannotti, M. Muller, Coexistence of very soft magnetism and good magnetoelastic coupling in the amorphous alloy $Fe_{62.5}Co_6Ni_{7.5}Zr_6Cu_1Nb_2B_{15}$, J. Magn. Magn. Mater. 215–216 (2000) 276–279, https://doi.org/10.1016/S0304-8853(00)00133-5.
[50] R. Germano, G. Ausanio, V. Iannotti, L. Lanotte, C. Luponio, Direct magnetostriction and magnetoelastic wave amplitude to measure a linear displacement, Sens. Actuators, A Phys. 81 (2000) 134–136, https://doi.org/10.1016/S0924-4247(99)00153-3.
[51] G. Ausanio, V. Iannotti, C. Luponio, L. Lanotte, R. Germano, A. D'Agostino, M. Inverno, R. Sorrentino, Potential application of innovative magnetoelastic resonators for vibration detection, Sens. Actuators, A Phys. 91 (2001) 123–125, https://doi.org/10.1016/S0924-4247(01)00474-5.
[52] L. Lanotte, G. Ausanio, V. Iannotti, G. Tomaiuolo, L. Lanotte, Torsional oscillation monitoring by means of a magnetoelastic resonator: modeling and experimental functionalization to measure viscosity of liquids, Sens. Actuators, A Phys. 295 (2019) 551–559, https://doi.org/10.1016/j.sna.2019.06.030.
[53] T. Drexel, G. Helmer, S. Garcia, G. Raveendran, Management of left main coronary artery obstruction after transcatheter aortic valve replacement utilizing a periscope approach, Catheter. Cardiovasc. Interv. 92 (2018) 1444–1448, https://doi.org/10.1002/ccd.27317.
[54] F. Nappi, C. Spadaccio, J.L. Sablayrolles, Delayed prosthesis malposition after transcatheter aortic valve implantation causing coronaries obstruction, Eur. J. Cardio-Thorac. Surg. 52 (2017) 1227–1228, https://doi.org/10.1093/ejcts/ezx266.
[55] N. Xu, S.H. Chen, X.Y. Xue, Q.S. Zheng, Y. Wei, T. Jiang, X.D. Li, J.B. Huang, H. Cai, Comparison of retrograde balloon dilatation and laparoscopic pyeloplasty for treatment of ureteropelvic junction obstruction: Results of a 2-year follow-up, PLoS One 11 (2016) 1–8, https://doi.org/10.1371/journal.pone.0152463.
[56] S. Inamdar, E. Slattery, R. Bhalla, D.V. Sejpal, A.J. Trindade, Comparison of adverse events for endoscopic vs percutaneous biliary drainage in the treatment of malignant biliary tract obstruction in an inpatient national cohort, JAMA Oncol. 2 (2016) 112–117, https://doi.org/10.1001/jamaoncol.2015.3670.
[57] M. Seyer-Hansen, A. Egekvist, A. Forman, M. Riiskjær, Risk of bowel obstruction during in vitro fertilization treatment of patients with deep infiltrating endometriosis, Acta Obs. Gynecol. Scand. 97 (2018) 47–52, https://doi.org/10.1111/aogs.13253.
[58] N. Gupta, C. Neeraj, B. Smriti, D. Sima, A comparison of the success rates of endoscopic-assisted probing in the treatment of membranous congenital nasolacrimal duct obstruction between younger and older children and its correlation with the thickness of the membrane at the Valve of Hasner, Orbit 37 (2018) 257–261, https://doi.org/10.1080/01676830.2017.1383483.
[59] S.B. Clayton, R. Patel, J.E. Richter, Functional and anatomic esophagogastric junction outflow obstruction: Manometry, timed barium esophagram findings, and treatment outcomes, Clin. Gastroenterol. Hepatol. 14 (2016) 907–911, https://doi.org/10.1016/j.cgh.2015.12.041.
[60] R. Berry, J.Y. Han, J.H. Tabibian, Difficult biliary cannulation: Historical perspective, practical updates, and guide for the endoscopist, World J. Gastrointest. Endosc. 16 (2019) 5–21, https://doi.org/10.4253/wjge.v11.i1.5.
[61] E. Parlak, A.S. Koksal, F. Kucukay, A.T. Eminler, B. Toka, M.I. Uslan, A novel technique for the endoscopic treatment of complete biliary anastomosis obstructions after liver transplantation: through-the-scope magnetic compression anastomosis, Gastrointest. Endosc. 85 (2017) 841–847, https://doi.org/10.1016/j.gie.2016.07.068.
[62] H. Park, A.H. Raffiee, S.W.M. John, A.M. Ardekani, H. Lee, Towards smart self-clearing glaucoma drainage device, Microsyst. Nanoeng. 4 (2018) 35, https://doi.org/10.1038/s41378-018-0032-3.
[63] R. Glaser, V. Caccese, M. Shahinpoor, Development of novel smart MR-gates for wireless dynamic control of fluid flow, Smart Mater. Struct. 22 (2013) 015012, https://doi.org/10.1088/0964-1726/22/1/015012.
[64] J. Chen, Q. Yu, X. Cui, M. Dong, J. Zhang, C. Wang, J. Fan, Y. Zhu, Z. Guo, An overview of stretchable strain sensors from conductive polymer nanocomposites, J. Mater. Chem. C. 7 (2019) 11710–11730, https://doi.org/10.1039/c9tc03655e.
[65] H. Wei, H. Wang, Y. Xia, D. Cui, Y. Shi, M. Dong, C. Liu, T. Ding, J. Zhang, Y. Ma, N. Wang, Z. Wang, Y. Sun, R. Wei, Z. Guo, An overview of lead-free piezoelectric materials and devices, J. Mater. Chem. C. 6 (2018) 12446–12467, https://doi.org/10.1039/c8tc04515a.

Vincenzo Iannotti is an associate professor of experimental physics at the Department of Physics 'E. Pancini' of the University of Naples Federico II, where he received his PhD in 1999. His research focuses on nanostructured magnetic materials (magnetic nanoparticles and their composites) and 2D materials (MXenes) for sensing and biosensing applications. The results of his research are reported in more than 100 publications in international peer-reviewed journals, in five publications in international scientific books, in a contribution to an Encyclopedia on Sensors, and in two patents.

Vincenzo Guarino is Research Director at IPCB-CNR in Naples. His main research interests include biomaterials, scaffold design and electrofluidodynamic technologies (i.e, electrospinning/spraying/atomization) for the fabrication of micro/nanostructured bio functional devices, particles and capsules for health/biomedical applications. He was appointed as PI of several international projects (international academies, research institutes, agencies and R&D companies) and member of scientific committees, project review panels and editorial boards of international journals. He is author/co-author of over 200 international publications on the material/biomaterials subjects. Since 2021, He was included in the World's Top 2% Scientists list by Stanford University ranking.

Iriczalli Cruz-Maya has a PhD degree in Engineering of products and industrial processes from the University of Naples Federico II. She won an Early-stage researcher position within the Marie Sklodowska-Curie Actions (MSCA) and worked as post doc scientist at CNR-IPCB. Cruz-Maya's research is focused on the development of scaffolds for tissue engineering and their in vitro biological characterization, the optimization of drug delivery systems via electrofluidodynamic technologies (EFDTs), in collaboration with R&D companies (i.e., Dompè). She is author/co-author of over 40 international publications (i.e., original papers, book chapters and proceedings) on the material/biomaterials subjects.

Zaheer Ud Din Babar completed his MS in Physics from the National University of Sciences and Technology (NUST), Pakistan in 2019. His master's research was focused on the synthesis and magnetic properties of Nb_2C MXene, and he reported its superconductivity. Since 2017, Zaheer has been actively engaged in MXene research and is currently a Ph.D. scholar at the Scuola Superiore Meridionale (SSM) of the University of Naples Federico II, Italy. His current research activities are centred on MXene synthesis, post-processing, and the development of MXene composites for sensing and biosensing applications.

Luca Lanotte is a researcher of the soft matter at INRAE since 2017. He obtained his PhD in Physics and Chemical Engineering in 2013 (Vinci Project 2009) with a project in collaboration between the University Federico II of Napoli (Italy) and the University of Grenoble (France). Currently, his research activity focuses on the study of the drying and the fouling in dairy mixes. To date, Luca has co-mentored six MSc students and two PhD students. He has co-authored 20 publications in peer-reviewed journals, 2 book chapters, and his works have been presented in more than 30 international/national conferences and meetings.

Luigi Ambrosio is Associate Senior Researcher at the Institute of Polymers, Composites & Biomaterials, National Research Council. He received the Doctoral Degree in Chemical Engineering, University of Naples Federico II. Qualified Full Professor in Bioengineering and in Materials Science and Technology. He received the ESB "G. Winter Award", for the high worldwide contribution to Biomaterials Science. He is Fellow of American Institute for Medical and Biological Engineering, Fellow of Biomaterials Science and Engineering, Fellow of the European Alliance for Medical and Biomedical Engineering & Science, and Member of the European Academy of Science. Publications include over 350 peer-reviewed journal articles.

Luciano Lanotte is a retired full professor of Experimental Physics from the University of Naples Federico II. Presently, he works as a senior research associate at the Institute for Polymers, Composites, and Biomaterials (CNR-IPCB) in Naples. With expertise in magnetoelastic effects, he directed the inaugural world conference on the topic (First MEA, Capri 1993) and organized numerous international schools and conferences on magnetism and sensing. Recognized with the 'Award as Valued Reviewer' in 2009 from Sensors and Actuators A. He taught at the Faculty of Engineering in Naples and the Aeronautical Academy in Pozzuoli.